2023

Potential Mechanism of 5-ALA treatment against Feline Infectious Peritonitis Virus Infection by Downstream Metabolite PPIX

Carissa V. Napier

POTENTIAL MECHANISM OF 5-ALA TREATMENT AGAINST FELINE INFECTIOUS PERITONITIS VIRUS INFECTION BY DOWNSTREAM METABOLITE PPIX

by

CARISSA TINA VANESSA NAPIER

SUBMITTED TO SCRIPPS COLLEGE IN PARTIAL FULFILLMENT OF THE DEGREE OF BACHELOR OF ARTS

PROFESSOR BETHANY CAULKINS
PROFESSOR ERIN JONES

DECEMBER 4TH 2023

Table of Contents

Acknowledgements

I would like to extend my thanks to my first reader, Dr. Bethany Caulkins, and second reader, Dr. Erin Jones. Both are professors whose classes I thoroughly enjoyed, and I am deeply grateful they accepted my requests to be my readers. Dr. Bethany Caulkins was a constant source of kindness and motivation throughout this semester. Her willingness to meet every week and provide feedback on my thesis gave me vital support and resources needed to complete this thesis. Thank you to all my professors who shaped my college experience. Special thanks to my mother Viola Napier and father John Napier, who have provided endless support in all my academic endeavors. Both of my parents consistently attended my extracurricular and academic events, and their unwavering dedication motivates me to be a better student and person. My father not only greatly engendered a curiosity for STEM in me at a young age, but also opened my eyes to the performing arts and music. Without his influence, I would not be the well-rounded individual I am today. I am sincerely grateful for my mother, who consistently displays her pride for me and always voices her support for my dreams. Her sincere love and gentle care for animals inspired me to pursue veterinary medicine. I would not be the woman I am today without her guidance and love. Thank you to my cousin Vanessa Riordan, and her husband Dan Riordan, who kindly housed me while I took organic chemistry in the summer. Lastly, I want to thank all my friends I have made over the years at the Claremont Colleges and from my hometown. You all have affected my life for the better and provided me with so many great memories that will be cherished forever. I cannot acknowledge you all, but to M. Downing, C. Briseño, L. Cursaro, E. de Castro, H. Downing, E. Schwerdfeger, K. Chaudhary, R. Braley, G. Foote, B. Beaston, C. Brunk, and F. Flores, I extend a vast amount of gratitude.

Abstract

Feline coronavirus (FCoV) infection is ubiquitous in domestic cats, and up to 12% of FCoV-infected cats may succumb to Feline Infectious Peritonitis (FIP). FIP is a highly lethal infectious disease caused by FIP virus (FIPV), the virulent biotype of FCoV. It is difficult to properly diagnose FIP, and to this date, there is no effective FCoV vaccine nor licensed therapeutic for FIPV. Considering the threat FIP poses to feline health, there is a demand from both owners and veterinarians for a proper therapeutic to effectively treat the infection. 5-aminolevulinic acid (5-ALA) is a highly bioavailable amino acid that is naturally synthesized in animal cells and has shown significant antiviral activity against coronaviruses SARS-CoV-2 and FIPV. The inhibition of FIPV infection is most likely due to the intracellular accumulation of a downstream metabolite called protoporphyrin IX (PPIX) from 5-ALA supplementation, which can bind to G-quadruplex (G4) structures in the viral genome and therefore inhibit viral translation and replication processes. This propositional study is designed to investigate the potential stabilization of G4s in FIPV by PPIX and its subsequent inhibition of the viral life cycle both *in vitro* and in feline cells.

Introduction

FIP

Feline Infectious Peritonitis (FIP) is an enveloped, single strand positive-sense RNA coronaviral disease. FIP virus (FIPV) is caused by a feline coronavirus (FCoV) which consists of two serotypes categorized based on the amino acid sequence of the spike (S) protein.[1] Infection rates of FCoV I are more common than FCoV II infection, with type I FCoV strains potentially being more likely to cause clinical FIP.[2] In spite of this, most research has focused on type II since it is readily propagated *in vitro*.[3] Within each serotype, there are two biotypes divided based on their pathogenicity: Feline enteric coronavirus (FECV) and FIPV.[4] FECV is an enteric form of FCoV that is ubiquitous in cats throughout the world and not in itself an important pathogen.[5] FIP virus (FIPV) is a virulent biotype of FCoV and arises during an *in vivo* infection of FECV from genetic mutations of the S protein.[6,7] FIPV and FECV differ substantially, with FECV proliferation confined to intestinal mucosal epithelial cells or mesenteric lymph nodes during natural infection, whereas FIPV infects feline peritoneal macrophages, conferring the ability for the virus to infect more types of cells, including monocytes, plasma cells, lymphocytes and neurocytes, thus producing high titers of progeny virus.[8] In effect, FIPV infects other types of cells continuously and more efficiently in comparison to its parent biotype.

Although cats of any age are susceptible to the virus, it is most prevalent among cats less than 3 years of age, especially from 4 to 16 months of age, followed by cats above 10 years of age.[8] There is some evidence indicating that the disease is associated with sex, but the closest related occurrence of FIP are factors such as high breeding density and an unsanitary breeding environment.[5,8] FIPV infection often occurs in catteries, shelters, kitten foster/rescue facilities, and dense free-roaming colonies, with kittens commonly becoming infected at around nine weeks of

age.[9] This aligns with the fact that FECV is shed in feces of most apparently healthy cats in large-multi-cat environments, efficiently spread and transmitted through direct ingestion of feces or contaminated litter and other fomites.[6,10] It is likely that the mutants of FECV capable of causing FIP are generated largely during the initial infection of FECV when levels of FECV replication are extremely high.[11]

Based on the disease characteristics, FIPV can be classified as effusive and non-effusive, or wet and dry peritonitis. Abdominal distension with ascites, dyspnea with pleural effusion, jaundice, hyperbilirubinemia, discernible masses on the kidneys and/or mesenteric lymph nodes, uveitis and a range of neurological signs associated with brain and/or spinal cord involvement are all common in cats with either the effusive or non-effusive forms of FIP.[9] Wet peritonitis is characterized by polyserositis, or the accumulation of thoracic and abdominal effusion, and vasculitis.[3] Dry peritonitis differs in its chronic progression, often taking several weeks to months for the characteristic granulomas in the organs to appear.[3,8] The mortality of the infection is extremely high once clinical signs appear, but some cats can live with the disease for weeks, months, or, rarely, years.[5,9] Resistance to FIP involves multiple factors, including genetic susceptibility,[11–13] age at the time of exposure,[14] and a number of stressors that occur at the same time of infection that may assert a negative impact on the ability of the cat to eliminate the virus, such as husbandry procedures the type of environment, and exposure to other infectious agents.[10,13,15,16] The time period between initial FECV exposure and clinical signs of FIP can vary, with some cats displaying symptoms in as short as two to three weeks, or as long as several months, or, even rarely, years. It is unconfirmed if this period reflects the time it takes for the mutant FIPVs to evolve, or for the disease to progress from a subclinical– which can either resolve or progress– to clinical state.[17,18] The clinical onset results in death, with a return to normal health being

extremely uncommon. In the rare event apparent recovery does occur, clinical signs recur months and even years later in some cats.[18] Younger cats and cats with effusive disease generally experience a shorter disease course between onset of clinical signs and death compared to older cats and cats with non-effusive disease.[9]

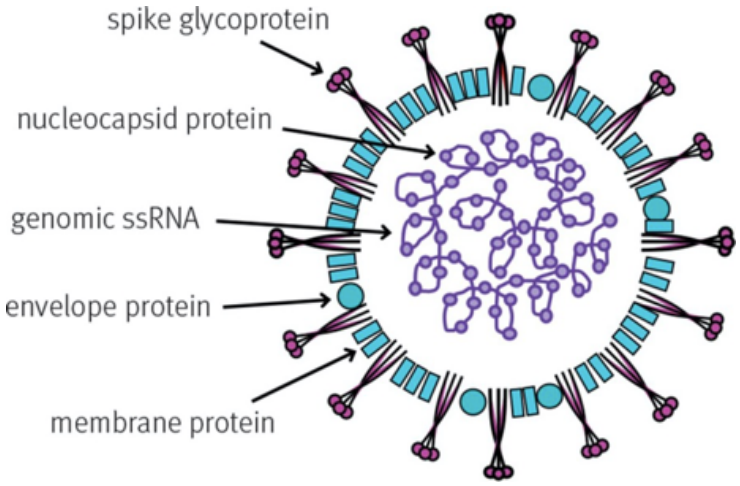

Figure 1. A feline coronavirus virion with relative position of structural proteins and genomic single-stranded RNA (ssRNA) indicated. Figure adapted from Barker et al. (2020).

The widely accepted theory for FIPV pathogenesis involves internal mutation. FIPV arises from internal mutation of endemic FECV, which occurs in approximately 1%-5% of enteric infections. This mutation confers the ability of the virus to infect blood monocytes and tissue macrophages.[7] The cell tropism transformation allows for productive infection of macrophages and blood monocytes, enabling systemic spread with concomitant immune-mediated events eventually leading to death.[7,11] To explain the mechanism behind internal mutation, research at the molecular and genetic levels has been conducted. In early studies, the 3c genes were observed to be complete in FECV, while more than two-thirds of the genes were mutated in FIPV, in which this mutant 3c gene is unable to produce an intact 3c protein. Although the prevailing view dictates that these mutations do not affect FIPV virulence, the 3c protein is essential for replication of FECV in the gut.[6] The loss of 3c function has been observed to be accompanied by mutations in

the S2 domain of the S protein.[19] Once the S gene is mutated, which allows the virus to infect macrophages and spread systemically, the accessory gene 3c becomes nonessential for replication.[6] This shift in the biotype and altered cell tropism of FECV allows for systemic spread of the virus, resulting in FIPV.[7,11]

The diagnosis or possibility of FIP is often met with reluctance from owners, due to the fact that most cats are reasonably well at the time of diagnosis, thus leading to a series of additional tests that claim to be highly specific and sensitive but might further cloud the diagnosis. Additionally, there exists a dearth of effective therapies, leading owners to research remedies and encounter anecdotal statements from owners who have found certain treatments to prolong life or even cure the disease.[9] However, considering the problems with interpreting FIP diagnostic tests, not all cats with a positive FIP test actually have the disease. If a cat has a self-limiting condition, they will appear to respond well to almost any non-harmful treatment that is administered, thus giving credibility to a particular treatment that deserves none.

Current FIP Therapeutics

Antiviral agents fall into two basic categories: one targets the cellular machinery that viruses seize and utilize for replication, and the other targets an activity specific to infection and/or replication.[3,9,20] Those which affect the cellular machinery tend to have a negative effect on both the host and virus, decreasing their efficacy.[5] Targeting specific regions of the viral genome that regulate essential pathways in infection or replication is a more effective and successful approach.[9] Recently, research has yielded promising results from FIPV drugs similar to those which have proven effective against HIV-1 and hepatitis C, which target specific proteins involved in RNA virus replication.[21] Remdesivir (GS-5374), an adenosine nucleoside monophosphate prodrug, is an antiviral drug developed specifically to work against emerging RNA viruses by inhibiting the

replication of several taxonomically diverse RNA viruses.[22,23] Remdesivir's more chemically simple parent nucleoside analog, GS-441524, was identified as a direct acting antiviral drug for FIPV.[21,24] Although its antiviral properties are incredibly promising, GS-441524 is expensive and currently unavailable for veterinary use. In response to the halted development of GS-441524, there is a growing at-home, unlicensed use of GS-441524-like drugs to cats who are suspected to have FIPV. Although these drugs are purported to be beneficial in treatment of FIPV-suspected cats, there still remains legal and medical risk.[25] Some owners have reported paying 10,000-20,000 USD for medication from these unlicensed sources, and the mean cost has been reported to be just under 5000 USD.[25] These data clearly indicate there is a large population of cat owners who become desperate to cure their fatally-ill cats once FIPV is suspected or diagnosed. The lack of an available, licensed antiviral therapy necessitates research on a safe, relatively cheap, and effective antiviral drug for FIPV.

G-Quadruplex Structures as Therapeutic Targets

DNA and RNA G4 structures are the result of specific G-rich sequence(s) forming G-tracts. Hoogsteen hydrogen bonding between neighboring G-tracts produces a square planar guanine tetrad (G-tetrad) or guanine quartet (G-quartet, Figure 2A). When two or more tetrads or quartets are able form a planar ring by stacking on top of each other, it forms a G-quadruplex (G4, Figure 2B). G4s are highly polymorphic structures, representing a huge family of stable structures with variations in strand stoichiometry, polarity, the length of loops, and their location in the sequence.[26,27] Generally, all G4 structures possess favorable thermodynamics, with RNA G4s exhibiting more stability than DNA G4s.[28,29] The unfolding kinetics of G4s are much slower than those of DNA or RNA hairpin structures, therefore, it is likely the formation of a G4 obstructs DNA and RNA metabolism.[28] From computational analysis of the human genome, putative G4-

forming sequences (PQS) were revealed mainly cluster in multiple highly conserved regions throughout the genome that are involved in replication and regulation of gene expression, such as telomeres, gene promoters, and DNA replication origins, strongly suggesting their role in these biological pathways.[30]

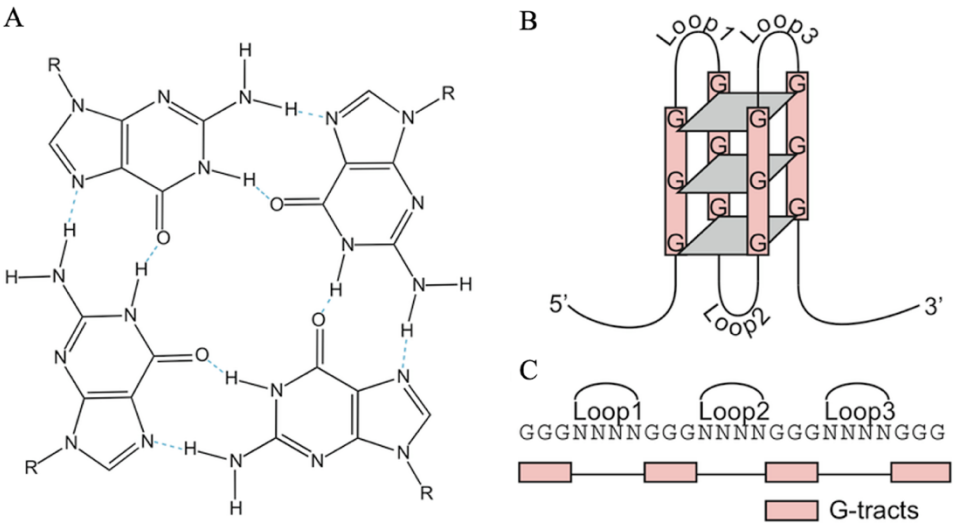

Figure 2. G-quadruplex (G4) structure and motif. A. Structure of a G-quartet. B. The planar ring formed by the stacking of G-tetrads or G-quartets. C. A general motif for G4 forming sequences. Figure adapted from Capra et al. (2010).

In addition to humans, PQS are found in other mammalian genomes, bacteria, and in viral genomes.[31] A recent plethora of research has suggested PQS can be involved in viral replication and recombination, virulence control, and the regulation of other pivotal viral life cycle steps.[27] Additional research has introduced the use of G4-forming oligonucleotides and G4 ligands as potential antiviral agents against multiple families of viruses.[27,32] In fact, a recent study on G-quadruplexes in SARS-CoV-2 has predicted many putative G4-forming sequences (PQSs) in the SARS-CoV-2 genome, and later Qin et al. (2022) confirmed several highly conservative and stable G4s in SARS-CoV-2 by multiple established characterization methods.[33,34] Furthermore, Qin et al. revealed that significant inhibition of both transcription and translation of the SARS-CoV-2 were achieved targeting the G4 sequences in SARS-CoV-2 with the established G4-stabilizer

TMPγP4. In addition, TMPγP4 displayed better antiviral activity than the FDA-approved COVID-19 therapeutic Remdesivir, suggesting that G4-stabilizers are promising, effective therapeutics against coronaviruses like FIPV.

5-Aminolevulinic Acid (5-ALA) and its metabolite, PPIX

5-aminolevulinic acid (5-ALA, Figure 3A), a precursor in the biosynthesis of tetrapyrroles such as protoporphyrin IX (PPIX, Figure 3B), is a natural amino acid that exists in animals, plants, fungi, and bacteria.[35,36] By utilizing the photosensitivity of PPIX, 5-ALA has been employed in photodynamic diagnosis and therapy for cancer in both dogs and humans, and additionally has been clinically used for metabolic improvement in diabetes, demonstrating the multi-beneficial applications of 5-ALA in human health.[37–39] Recent studies have revealed the in vitro antiviral effects of 5-ALA against Classical Swine Fever Virus, as well as positive-sense coronaviruses Feline Infectious Peritonitis and SARS-CoV-2, but the exact antiviral mechanism has not yet been elucidated.[40–42]

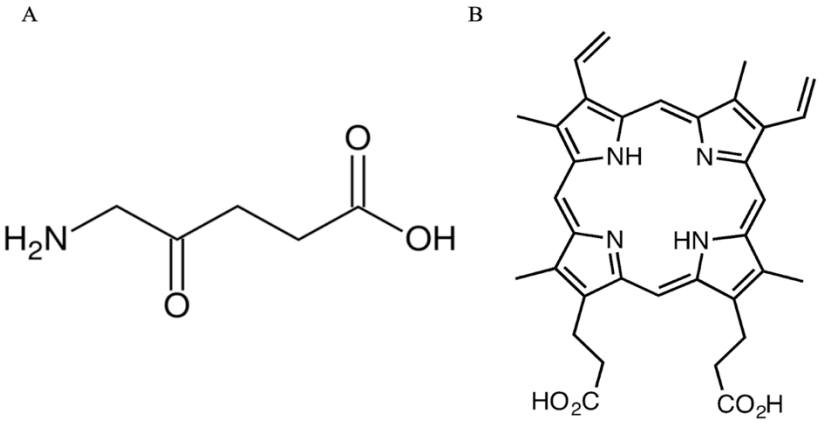

Figure 3 A. Structure of 5-aminolevulinic acid (5-ALA) B. Structure of protoporphyrin IX (PPIX).

Multiple studies have reported the antiviral effects of PPIX against pathogens such as Dengue virus, vesicular stomatitis virus, Zika virus, influenza A virus, and SARS-CoV-2.[43–47]

Although PPIX presents a promising treatment for coronaviruses such as FIPV, it displays poor bioavailability as a result of its inefficient uptake in the intestine and incorporation into cells, therefore the practical medicinal use of PPIX is not realistic.[48] A recent study reported that 5-ALA significantly inhibits FIPV infection in feline kidney cells.[41] However, the mechanism by which FIPV infection was inhibited was not investigated further. Notably, a study investigating the antiviral effects of 5-ALA against Classical Swine Fever Virus observed that the intracellular accumulation of PPIX by 5-ALA treatment played the key role in the antiviral mechanisms of 5-ALA, suggesting that 5-ALA can be utilized as an oral medicine or supplement to provide PPIX required for infection inhibition.[40] The proposed mechanism behind PPIX antiviral activity is its potential to stabilize G4-structures in the virus genome, since PPIX is an established G4 ligand.[26] The demonstrated antiviral activity of 5-ALA in FIPV necessitates research to identify and validate G4-forming sequences in the FIPV genome, and evaluate if PPIX exerts a stabilizing effect on these sequences. Further investigation into if PPIX is inhibiting the viral replication and/or translation processes can establish 5-ALA as an effective therapeutic for FIPV and open up further avenues to investigate its antiviral potential in live cats.

Experimental Proposal

The severity of FIPV diagnoses in cats necessitates a treatment that can effectively reduce viral infection. Along with demonstrating that 5-ALA and PPIX affect replication of live FIP virus, the main focus of this study will be uncovering the antiviral mechanism that 5-ALA exerts, possibly by stabilizing the G4 structures in the FIPV genome through the downstream metabolite PPIX. Not only will this research boost the possibility of 5-ALA as an effective therapeutic for cats with FIPV, but also contribute research into the novel field of G4s as a drug target against coronaviruses like FIPV.

Aim 1: Identify and validate PQS in the FIPV genome and demonstrate that PPIX binds and stabilizes a representative G4-sequence

First and foremost, potential G-quadruplex forming sequences (PQS) in the FIPV genome will be identified and validated through a multitude of established methods. Considering studies have reported their presence in SARS-CoV-2 among many other viral genomes, it is likely the FIPV genome possesses a number of PQS.[27,34,49,50] Several algorithms have been developed to identify sequences with the potential to form G4s and have previously shown success in identifying G4s that are likely to form in RNA.[51,52] Along with computational screening of the FIPV (strain WSU-II 1176) genome, the PQS identified will be subject to *in vitro* screening techniques to confirm their formation along with their stability under physiological conditions. It is expected that a number of PQS will be identified, and at least one PQS will demonstrate great stability and will be chosen as the representative to investigate the behaviors of G4s in FIPV.

To examine if PPIX can bind and stabilize the representative G4 sequence, circular dichroism (CD) spectra and CD thermal melting analysis will be conducted with the representative

PQS in the presence of PPIX. These spectra results should indicate that PPIX can bind and stabilize the chosen PQS. A mutant (G/A mutations) PQS will also be subjected to the same assays to serve as a negative control, since the mutations will disrupt the ability for the G4 to form. We should observe no G4 formation nor stabilization by PPIX with the PQS mutants.

Aim 2: Examine the inhibitory function of G4s on FIP virus life cycle and the ability of PPIX to enhance this function via G4-specific stabilization.

If the most stable PQS(s) are located in the open-reading frames (ORFs) of FIPV, experiments are needed to investigate the possible inhibition of translation of viral RNA by the G4s in this location. To this end, *in vitro* translation (IVT) assays will be performed in the absence or presence of PPIX at increasing concentrations to evaluate the extent to which G4 formation inhibits translation of the wild type (denoted as X4-WT) or mutant (X4-Mut) PQS. Additionally, to examine the protein expression in living cells, the same sequences encoding X4-WT or X4-Mut will be cloned into a vector and transfected into Crandell Rees Feline Kidney (CRFK) cells. Finally, to investigate if G4 formation inhibits viral RNA replication by sterically inhibiting the FIPV RNA dependent RNA polymerase (RdRp), a cell-based RNA replication assay will be performed with treatments of PPIX at increasing concentrations in CRFK cells. The results of these assays will ultimately provide evidence for the potential inhibition of viral protein expression and viral RNA replication by PPIX.

Aim 3: Evaluate the effects of PPIX and 5-ALA on the replication of live FIPV

Lastly, assays will be performed on FIPV-infected CRFK cells to confirm the antiviral effect of 5-ALA and PPIX. Before carrying out these experiments, a cytotoxicity assay will be used to assess the cytotoxic effects of 5-ALA and PPIX in CRFK cells, and these results will be

used as a guide to determine the treatment concentrations for further experiments. Two assays will be utilized to confidently confirm the antiviral effects of our compounds: RT-qPCR of viral RNA and quantification of the viral titers by the median tissue culture infectious dose ($TCID_{50}$). In each of these assays, infected cells will be treated with 5-ALA or PPIX and cell supernatant will be collected and subsequently analyzed.

Finally, we will validate that 5-ALA treatment is inhibiting FIPV infection by PPIX binding the FIPV genomic RNA G4s. First, an immunofluorescence assay employing a DNA/RNA G-quadruplex antibody will affirm the formation of viral G4 structures during viral replication. Then, locked nucleic acid (LNA) antisense oligonucleotides (ASOs) complementary to FIPV G4s will be used to "open" G4 structures in FIPV cells incubated with PPIX. Subsequent RT-qPCR of viral RNA and quantification of the viral titers by the $TCID_{50}$ will be carried out with the hypothesis that 5-ALA and PPIX's antiviral effects are negated by the destabilization of the G4s.

Methods and Materials

Cell cultures, Viruses, Oligomers, and Reagents

Crandell Rees feline kidney (CRFK) (ATCC, USA) cells will be grown in Eagles' Minimum Essential Medium (MEM) containing 50% Leibovitz's L-15 medium, 5% fetal calf serum (FCS), 100 U/ml of penicillin, and 100 μg/ml of streptomycin. Cells will be incubated at 37°C and 5% CO_2. Maintenance of CRFK cells will be carried out in the same composition as the growth medium with only 2% fetal calf serum. Cell culture-adapted feline coronavirus WSU 79-1146 (GenBank DQ010921), also known as FIPV I WSU 79-1146, will be obtained from ATCC. FIPV I WSU 79-1146 is the model strain for *in vitro* FCoV study.[53] Wild-type RNA of each PQS and mutant PQS RNA (G/A mutations) will be ordered from Sigma of HPLC-purified grade. 5-ALA, PPIX, and TMPγP4 will be obtained from Sigma Aldrich. GS-44154 will be bought from MCE. For IVT assays and CD spectra, PPIX will be dissolved in DMSO and TMPγP4 will be dissolved in water to the desired concentrations. For the cell-based assays, all compounds will be dissolved in maintenance medium to the desired concentrations.

Bioinformatics analysis

The complete genome of FIPV I WSU 79-1146 will be retrieved from the NCBI Genome database (http://www.ncbi.nlm.nih.gov/nuccore/NC_002306.3). The FASTA sequences of the FIPV I genome will be used for the prediction of the putative G4-forming sequences with QGRS-mapper.[54] The search is based on the following motif:

$G_{\geq 2}N_{1\text{-}15}G_{\geq 2}N_{1\text{-}15}G_{\geq 2}N_{1\text{-}15}G_{\geq 2}$

In which G corresponds to guanine and N corresponds to any base including guanine. Then, to evaluate the G4 folding capabilities, the consecutive G over consecutive C ratio (cGcC) 49, G4Hunter (G4H), and G4 neural network (G4NN) scores will be assessed by the G4RNA screener (http://scottgroup.med.usherbrooke.ca/G4RNA_screener/).

cGcC is employed to address the concern of competition between G4 and Watson-Crick based structures.[55] This ratio considers the presence of cytosine runs in the vicinity of a potential G4, as base pairing of those C runs with G runs can hinder potential G4 formation. Here, a ratio value greater than the set, arbitrary threshold of 4.5 will be considered as being accessible under conditions favoring G4 formation.

G4H is designed similarly to the cGcC score but analyzes DNA sequences. Each contiguous G receives an increasing positive score, and each contiguous C receives an increasing negative score.[56] The average of these values gives a score, and in this study, PQSs with a ratio value above the arbitrary threshold of 0.9 will be considered favorable.

G4NN evaluates the similarity of a given sequence to known G-quadruplexes and reports it as a score between 0 and 1.[51] In this study, PQSs with a ratio value superior to the arbitrary threshold of 0.5 will be considered favorable.

Circular dichroism spectroscopy and thermal denaturation analysis

Circular dichroism (CD) experiments will be performed using 4μM of the relevant RNA sample in 50 mM Tris–HCl (pH 7.5) buffer either in the absence of salt, or in the presence of 100 mM of either LiCl, NaCl or KCl. Before taking the CD measurement, each sample will be heated at 70°C for 5 minutes and then slow-cooled to room temperature over a one-hour period by a Thermal Cycler (Thermo Fisher Scientific). Using a Jasco J-810 spectropolarimeter equipped with a Jasco Peltier temperature controller in a 1 mL quartz cell cuvette with a path length of 1 mm. CD

scans, ranging from 220 to 320 nm, will be recorded at 25°C at a scanning speed of 50 nm/min with a two second response time, 0.1 nm pitch, and 1 nm bandwidth. The CD data will represent the average of three wavelength scans. A control experiment will be performed in the absence of RNA.

CD thermal denaturation will be performed using the same setup. CD spectra will be measured at a wavelength ranging from 220 to 320 nm, with a scanning speed of 50 nm/min, and a temperature ranging from 25 to 95 °C at intervals of 1 °C. Molar ellipticities of the indicated wavelength at 25 and 95 °C will be set as 100% and 0%, respectively. The normalized molar ellipticities will be fitted using GraphPad Prism 7 software (GraphPad Inc.). The T_m values will be recorded as the temperatures at which the normalized molar ellipticity is 50%. The CD thermal denaturation data will represent the average of three wavelength scans. A control experiment will be performed in the absence of RNA. To examine G4-ligand enhanced thermal stability on our G4, CD spectroscopy will be carried out with 1.0 μM PPIX or TMPγP4, and CD thermal denaturation will be carried out with 1.5 μM PPIX or TMPγP4.

Nondenaturing polyacrylamide gel electrophoresis experiments

Native gel electrophoresis will be performed by acrylamide gel (15%) and run at room temperature, using a 1X TBE buffer containing 10 mM KCl. The gel will be silver stained. About 2 μM RNAs will be loaded on the gel.

^{1}H NMR spectroscopy

^{1}H NMR spectra will be carried out on a Bruker Avance III 500 MHz NMR Spectrometer. The RNA samples will be dissolved in 10 mM phosphate-buffered saline (PBS) (pH 7.0) containing 100 mM KCl and 10% D2O at a final concentration of 0.3 mM in strand.

Stopped-flow experiments

To screen the stable G4s *in vitro*, N-methyl mesoporphyrin IX (NMM), a well-known G4-specific ligand, will be used.[57] Fluorescence stopped-flow experiments will be carried out by using an Agilent Cary spectrophotometer with a SFA-20 accessory. NMM treated samples (NMM/F-PQS-WT or NMM/F-PQS-Mut in 10 mM Tris-HCL buffer, 0 mM KCl, pH = 7.2) will be mixed with K^+-containing buffer (10mM Tris-HCL buffer, 200 mM KCl, pH =7.2). The concentration of NMM and the RNA oligos will be fixed at 1 μM. Fluorescence changes will be monitored at a wavelength of 661 nm with an excitation wavelength of 395 nm, as done previously.[34]

Immunofluorescence Assays

BG4 specific antibody (anti-DNA/RNA G-quadruplex (and related small molecules) (BG4) Standard Size Ab00174-1.6) will be purchased from absolute antibody. Cells will be washed twice in 1X PBS, fixed with 4% paraformaldehyde for 10 minutes, permeabilized with 0.5% Triton X-100-PBS for 15 minutes, incubated after with 100 mg/mL RNase A for one hour at 37 °C, and then blocked for 30 minutes with 3% BSA-0.2% Triton X-100-PBS. Then, cells will be simultaneously incubated with BG4 specific antibody and viral RNA FISH probes for 16 hours at 4 °C. Fluorescent secondary antibodies will be used in a 1:1000 dilution for 45 minutes at 37 °C. DAPI will be incubated for two minutes in the dark before taking images with a confocal laser-scanning microscope.

In Vitro Translation (IVT) Assays

To generate the FIPV transcripts with the G4 site needed, pGEM-T Easy Vector (Promega) constructs that encode the FIPV genome sequence(s) with the G4 site(s) or mutant G4 site(s) will be created with a Flag tag at the C-terminus. Mutations will be achieved using the Stratagene

QuikChange Site-Directed Mutagenesis kit. Following PCR amplification, these transcripts will be transcribed and translated using TNT® Quick Coupled Transcription/Translation System (Promega). Reaction contents will be subjected to SDS-PAGE and proteins will be detected by Bradford assay (Bio-Rad)**.** IVT assays will be performed with PPIX or TMPγP4 in concentrations of 0, 1.25, 2.5, 5, or 10 μM.

To assess the translational efficiency of the FIPV genome sequence(s) with the G4 site(s) or mutant G4 site(s) in CRFK cells, the FIPV I WSU 79-1146 genome sequences with our WT- and mutant G4 sites will be PCR-amplified and subcloned into a pCAG-Flag vector. By using the Stratagene QuikChange Site-Directed Mutagenesis kit, we will point mutate the G4 site to produce the mutant G4 sites. These plasmids will be transfected into CRFK cells using Lipofectamine 3000 (Invitrogen), following the manufacturer's protocol. Cells will be treated with PPIX or TMPγP4 in concentrations of 0, 1.25, 2.5, 5, or 10 μM, and will be harvested after 48 to 72 hours. Lysates will be subjected to SDS-PAGE and a Western blot will be performed.

RNA Replication Assay

A reporter vector will be generated to encode the FIPV I WSU 79-1146 genome sequence for nsp12, the non-structural protein which forms the RNA dependent RNA polymerase (RdRp).[58] The FIPV I WSU 79-1146 nsp12 gene will be PCR-amplified and subcloned into pCAG-Flag vector. To generate the FIPV transcripts with G4 site for RNA replication assays, a sequence encoding the 5′ untranslated region (UTR)-G4 -3′UTR will be first synthesized, then inserted into a pGEM®-T easy vector system (Promega). The FIPV RNA with G4 site will be produced using T7 RNA polymerases from a standard in vitro transcription kit. Cells will be transfected with the nsp12 and G4 plasmid at a 10:1 ratio using Lipofectamine 3000 (Thermo Fisher Scientific). At 12 hours post transfection, cells will be re-seeded in 24-well plates (4×10^4/well) and treated with

PPIX or TMPγP4. After 48-hour incubation, cells will be collected and measured for RNA levels by RT-qPCR assays.

Cytotoxic Effects of Compounds

Cytotoxicity of 5-ALA, PPIX, TMPγP4, and GS-441524 will be assessed using a commercially available procedure (CellTox Green Cytotoxicity Assay, Promega). Cytotoxicity will be quantified by the intensity of fluorescence as the dye selectively binds the DNA of apoptotic/necrotic cells. CRFK cells will be seeded in 96-well plates at an initial density of 1×10^5 cells/well in 200 µL medium. After 24-hour incubation at 37 °C in a humidified 5% CO2 environment, 100 µL of cell suspension will be treated with 50 µL of 1000, 750, 500, 250, and 0 µM concentrations of 5-ALA, PPIX, or GS-441524 in the appropriate wells, and allowed to incubate for 24 hours. After incubation, 100 µL CellTox™ Green Reagent (2X) will be added per well, with subsequent mixing by orbital shaking (700–900 rpm) for one minute to ensure homogeneity. After a 15-minute incubation period at room temperature, shielded from ambient light, fluorescence will be measured at 450 nm using a 96-well spectrophotometric plate reader, as described by the manufacturer. Absorbance of formazan will be compared to untreated CRFK cells (negative control), and cells treated with a cell lysing reagent provided by the manufacturer (positive control). Percentage cell viability will be calculated using the following formula:

Cell viability (%) = [(OD of compound-untreated cells - compound-treated cells)/ (OD of compound-untreated cells)] × 100

The 50% cytotoxicity concentration (CC_{50}) will be defined as the cytotoxic concentration of each compound that reduced the absorbance of treated cells to 50% when compared with that of the untreated cells.

FIPV-79-1146 inoculum and viral titer/plaque inhibition assay

Crandell-Rees feline kidney (CRFK) cells will be propagated in 250 mL flasks with 25 mL DMEM/10%FBS and infected at 70% confluency with 1 mL cell-culture supernatant containing 5 × 10^5 median tissue culture infectious doses ($TCID_{50}$) per mL of serotype II FIPV WSU-79-1146 and incubated for 48 hours. Flasks will be frozen at −70 °C for eight minutes and the thawed mixture of cells and original culture fluid will be centrifuged to remove cellular and subcellular debris and supernatant stored in liquid nitrogen. CRFK cells will be seeded in 96 well plates and then inoculated with 1 mL/well of a serial 10-fold dilution (10^{-1}-10^{-12}) of the frozen infected supernatant. Plates will be incubated for 48 hours, stained with crystal violet, and each well will be scored for cytopathic effect (CPE). A $TCID_{50}$ will be calculated from three replicates by the Reed-Muench method.

To determine the half maximal effective concentration (EC_{50}) of our proposed antiviral compounds, the CRFK cells will be grown in 24 well plates. Cells will be pre-treated with the different doses of the indicated antiviral compounds for 48 hours at 37°C. Following 48-hour incubation, cells will be inoculated with 1 × 10^4 $TCID_{50}$ for one hour at 37°C. The excess virus inoculum will be removed by washing three times with PBS. Then, 200 µL of maintenance medium (DMEM/2% FBS) will be added to each well, and the cells will further culture for 48 hours. The cells will be observed daily for CPE, and the $TCID_{50}$ value will be calculated with the Reed-Muench method. The EC_{50} will be defined as the effective concentration of compounds that reduced the virus titer in the culture supernatant of infected cells to 50% when compared with that of the virus control.

Simultaneous immunofluorescence of BG4 and fluorescence in situ hybridization (FISH)

BG4 specific antibody (anti-DNA/RNA G-quadruplex (and related small molecules) (BG4) Standard Size Ab00174-1.6) will be purchased from absolute antibody. Stellaris FISH probes will be bought from Biosearch Technologies. Cells will be washed twice in 1× PBS, fixed with 4% paraformaldehyde for 10 minutes, permeabilized with 0.5% Triton X-100-PBS for 15 minutes, incubated after with 100 mg/mL RNase A for 1 h at 37 °C, and then blocked for 30 minutes with 3% BSA-0.2% Triton X-100-PBS. Then, cells will be briefly incubated with BG4 specific antibody (1:400) and viral RNA FISH probes (1:1000) in Hybridization Buffer consisting of 20 μg/mL fish sperm DNA (fsDNA), 50 μg/mL heparin, 50% Deionized formamide, 0.1% SDS, 5 × Denhardt's and 5 × SSC (PH = 7.0) for at least 4 hours at 37 °C. Slides will be washed three times and then incubated with fluorescent secondary antibodies will be used in a 1:1000 dilution for one hour at 37 °C. Finally, slides will be washed three times and DAPI will be incubated for two minutes in the dark before taking images with confocal laser-scanning microscope.

Antisense oligonucleotides assays

All the locked nucleic acid (LNA) antisense oligonucleotides (ASOs) targeting the FIPV G4s will be synthesized by Sigma-Aldrich. For ASOs treatment, CRFK cells will be pre-transfected with a mixture of 17-mer ASOs targeting the G4s or a random 17-mer ASO for 6 hours prior to virus infection and PPIX treatment. At 72 hours post infection, cell supernatant will be collected for RT-qPCR and viral plaque inhibition assays.

Quantitation of FIPV replication by RT-qPCR

Viral RNA will be isolated from both the culture supernatant (QIAamp Viral RNA Mini Kit (Qiagen) and pelleted cells (RNAeasy, Qiagen) according to the manufacturer's instructions. DNase treatment of isolated RNA will be accomplished with TURBO DNase (Ambion). RNA will

be reverse transcribed into cDNA with the Origene First-Strand cDNA Synthesis System for RT-PCR (Origene). A control reaction excluding reverse transcriptase will be included for each sample. FIPV RNA copy numbers will be measured by RT-qPCR. PCR primers will be based on a consensus sequence of the feline coronavirus 7b gene.[24] A control reaction excluding cDNA (water template) will be included for each assay. Quantitative PCR for the GAPDH housekeeping gene will be performed in parallel and results will be normalized per 10^6 copies of GAPDH. Quantification of FIPV RNA copy number will be based on a standard curve generated from viral transcripts prepared by *in vitro* transcription of a plasmid (pCR2.1, Invitrogen) containing a 112 nucleotide-long amplicon.

Western blotting assays

For protein analysis of whole-cell lysates, cells will be briefly lysed in RIPA (Thermo Fisher Scientific) buffer. Total proteins (10 - 20 μg) will be re-suspended in Laemmli buffer (63 mM Tris-HCl, 10% glycerol, 2% SDS, 0.0025% bromophenol blue, pH 6.8) and electrophoresed on SDS-polyacrylamide gels. Then, proteins will be transferred to a polyvinylidene difluoride membrane. After an incubation with antibodies specific for Flag (Invitrogen) or GAPDH (Invitrogen), the blots will be incubated with anti-mouse for FLAG and GAPDH (Invitrogen) secondary antibodies conjugated to horseradish peroxidase. The immunoreactive bands will be detected using SuperSignal™ West Pico chemiluminescent substrate kit (Thermo Fisher Scientific) and Western blotting detection system (BioRad). GAPDH will be used as a loading control for western blotting assays.

Expected Results

Bioinformatics analysis was carried out using G4RNA screener, resulting in the identification of 24 PQS in the positive strand of FIPV WSU 79-1146. Thirteen of these PQS displayed one or more scores above the thresholds set (Table S1). Several methods will be employed to characterize the G4 formation and stability of each of these thirteen PQS (Figure 4A-E). At least one of these PQS should display stability in physiological conditions. It is likely the chosen PQS will reside in the ORFs 1a or 1b, as more potential stable G4s were identified in the ORFs in comparison to the structural genes.

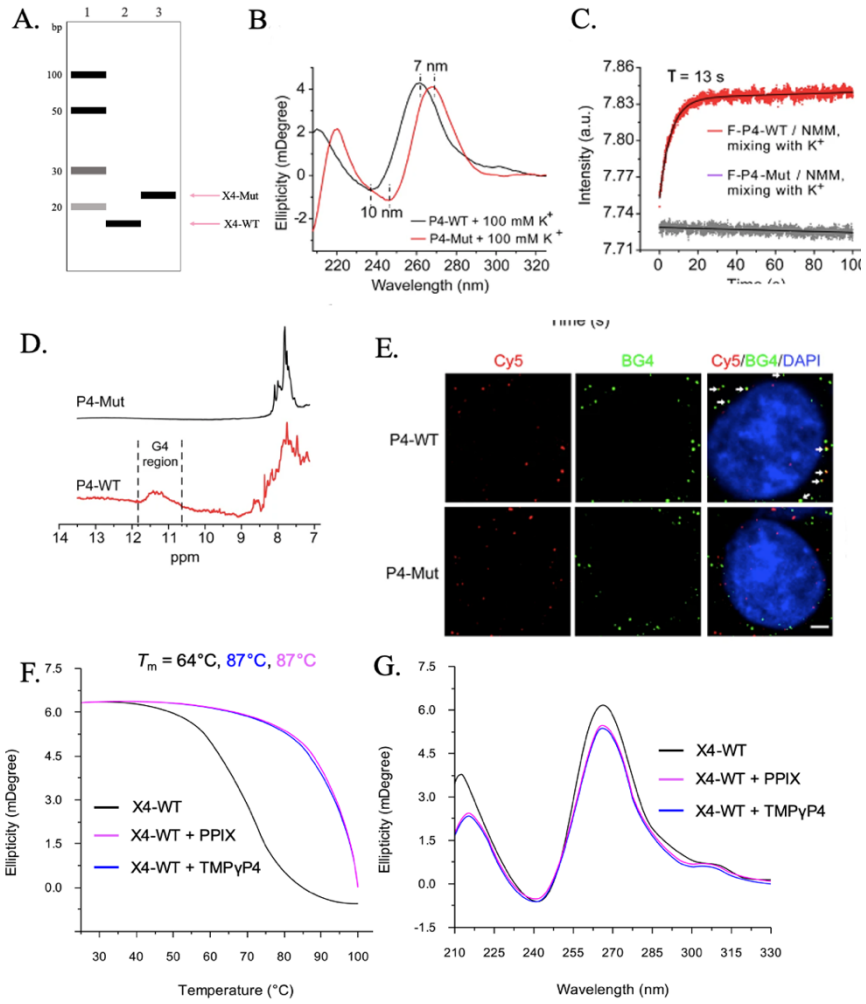

Figure 4. Characterization of the representative G4 formation and stabilization by PPIX. A. The formation of X4 G4 detected by nondenaturing polyacrylamide gel electrophoresis (PAGE) experiments. Lane 1, DNA ladder; Lane 2, X4-WT; Lane 3, X4-Mut. B. CD spectroscopy of X4-WT and X4-Mut. C. The kinetic folding process of X4 G4 detected by the stopped-flow assays. D. The formation of X4 G4 detected by ^{1}H NMR. E. The formation of X4 G4 in live cells detected by immunofluorescence assays employing BG4 antibody. Left, the white arrows indicated the colocalized foci of Cy5-labeled RNA (red) with BG4 (green). Scale bars, 4 μM. Right, Cy5/BG4 foci number was quantified. ****P < 0.0001. F. Projected CD thermal melting curves of X4-WT (1.5 μM) with PPIX (1.5 μM) or TMPyP4 (1.5 μM). G. Projected CD spectroscopy of X4-WT (1.0 μM) without or with PPIX (1.5 μM) or TMPyP4 (1.5 μM). Figures B-E were adapted from Qin et al. (2022).

A stable G4 sequence will be chosen if the various *in vitro* characterization assays display results similar to the characterization of a stable G4 sequence named

"P4" in the SARS-CoV-2 genome (Figure 4A-E).[34] Once a representative G4-forming sequence is chosen, the CD thermal denaturation analysis and CD spectroscopy will be performed in the presence or absence of PPIX. TMPγP4 will be used as a positive control, since it has displayed a strong ability to bind SARS-CoV-2 G4s.[34] Considering that PPIX is an established G4-specific ligand, it is expected that it will significantly enhance the thermal stability of the chosen G4, denoted as X4 (Figure 4F), thus demonstrating there are strong interactions between the G4 and PPIX. The CD peak of the G4 should not change in the presence of any of the molecules, as binding by the ligands is not expected to destroy the structure of the G4 (Figure 4G). With these results, a stable G4 will be identified and PPIX will be confirmed to bind and stabilize the representative G4.

Following the verification of G4 formation and stabilization by PPIX in the FIPV genome, the function of the representative G4 in the viral life cycle will be examined. If the most stable G4 is located in the ORFs, we want to

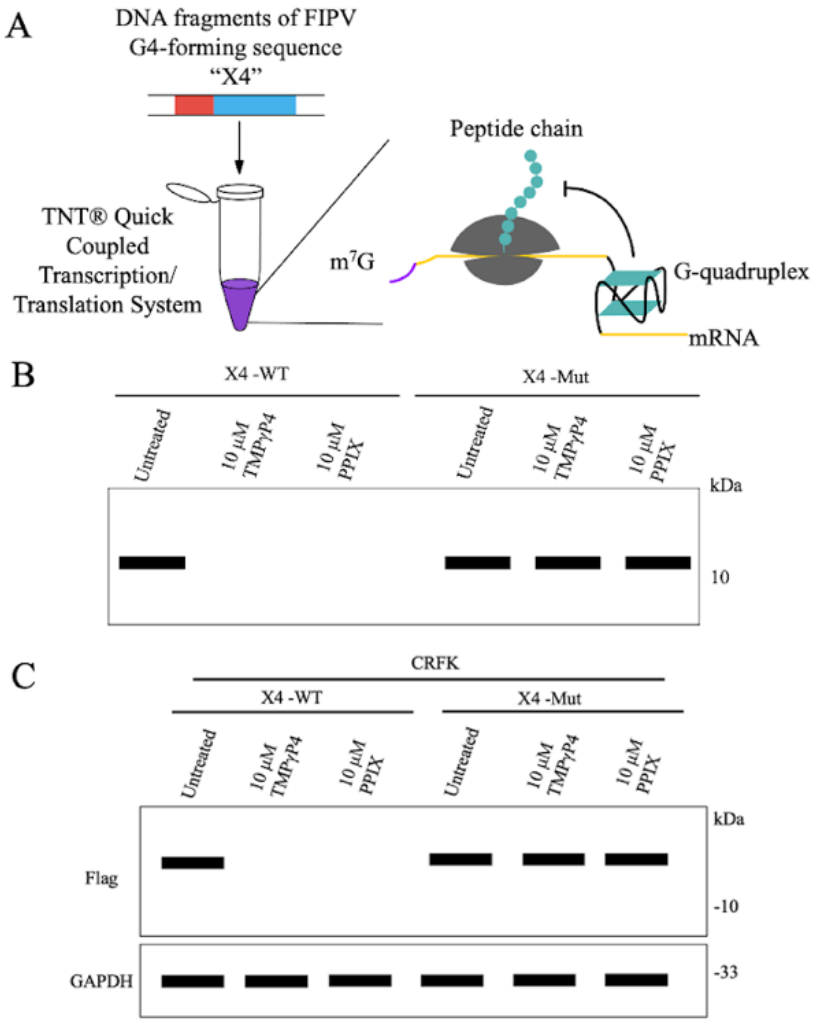

Figure 5. PPIX inhibits FIPV viral RNA translation in vitro and in cells in a dose-dependent manner. A. In vitro translation (IVT) schematic. B. PPIX or TMPγP4 treatment inhibits the translation of mRNA in X4-WT in IVT assays. C. PPIX or TMPγP4 treatment inhibits the translation of X4-WT mRNA in CRFK cells. Results from gels will be assessed using Image J software.

confirm that inhibition of translation of the viral proteins by G4 formation and stabilization by PPIX in the FIPV genome, the function of the representative G4 in the viral life cycle will be examined. If the most stable G4 is located in the ORFs, we want to confirm that inhibition of translation of the viral proteins by G4 formation is occurring. From *in vitro* translation (Figure 5A), we expect that in the presence of PPIX, translational efficiency will be lower in the X4-WT than in the X4-Mut as a result of G4 formation inhibiting translation (Figure 5B). Results from CRFK cells should be consistent with the IVT assays. The translation of X4-WT should be less than that of X4-Mut, and PPIX should decrease the protein levels of X4-WT in a concentration-dependent manner (Figure 5C, projected results from the 10 μM treatment are shown).

After the FIPV viral replicase complex is assembled, FIPV negative-strand intermediates are synthesized by positive strand RNA. Since the RNA-dependent RNA polymerase (RdRp) is an essential enzyme involved in viral replication,[59] and can be inhibited by the steric hindrance caused by G4s during the elongation phase of RNA synthesis,[60] it is expected that G4 formation

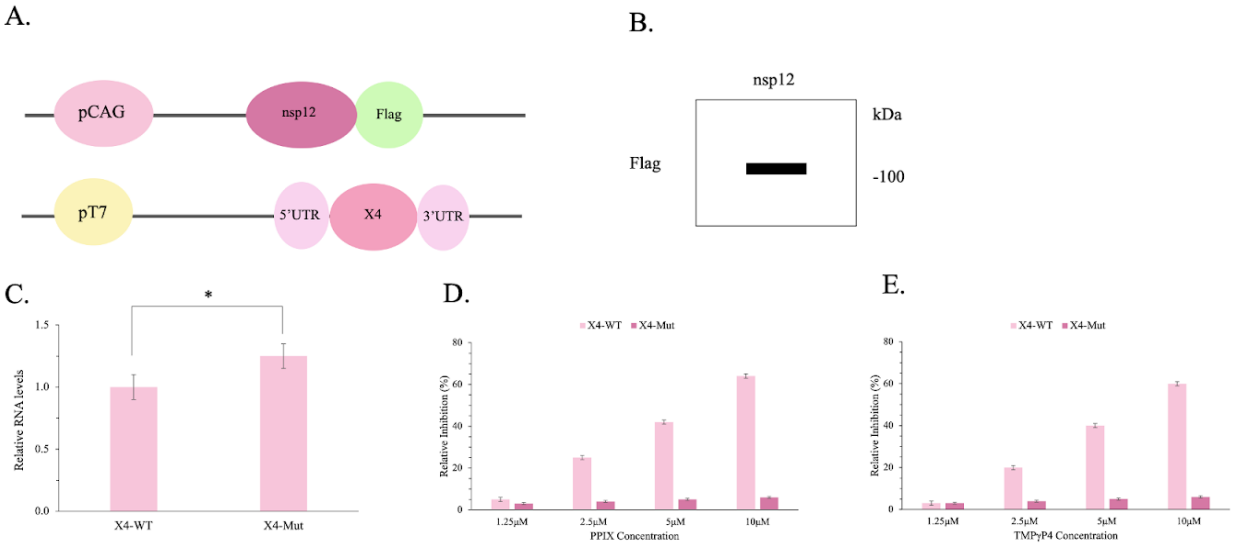

Figure 6. **PPIX inhibits FIPV RNA replication in a dose-dependent manner.** A. The expression vectors of the FIPV RNA-dependent RNA polymerase complex (nsp12). The pGEMT vector carrying X4 sequences fused to FIPV 5'UTR and 3'UTR. B. The protein expression of nsp12 in transfected CRFK cells. C. The formation of a G4 inhibits the replication of RNA in CRFK cells. D. PPIX E. or TMPγP4 inhibits the replication of RNA of the G4 in CRFK cells in a dose-dependent manner. RNA levels quantified by RT-qPCR. Data are shown as means ± SEM of three independent experiments, two-tailed Student's t-test. **P < 0.01, ***P < 0.001, ****P < 0.0001.

and stabilization by PPIX will inhibit FIPV RNA replication. To investigate this hypothesis, cell-based RNA replication assays[61,62] employing a plasmid encoding FIPV RdRp (nsp12) and an expression vector yielding our G4-forming sequence will be performed (Figure 6A). If the hypothesis is correct, X4-WT should have lower RNA levels than X4-Mut (Figure 6C), and stabilization by PPIX should inhibit the replication of X4-WT in a dose-dependent manner (Figure 6D). If the results appear similar to the projected results presented here, it will indicate that G4 formation in FIPV inhibits both the viral replication and translation processes. Additionally, it will demonstrate if PPIX can further inhibit the viral replication process by stabilizing the G4 regions in the FIPV genome.

Next, the effects of 5-ALA and PPIX on the replication of live viruses will be evaluated. First, determining the toxicity of our compounds is a prerequisite to all other assays, since the 50% cytotoxic concentrations (CC_{50}) will be used for determining the concentrations used in the following assays. Using the CellTox Green Cytotoxicity Kit, CRFK cells will be treated with varying concentrations of our compounds for 24 hours and the percent cell viability will be calculated (Figure 7). The positive control, GS-441524, should not display any cytotoxicity as demonstrated by past research.[24,34] 5-ALA should display minimal toxic effects

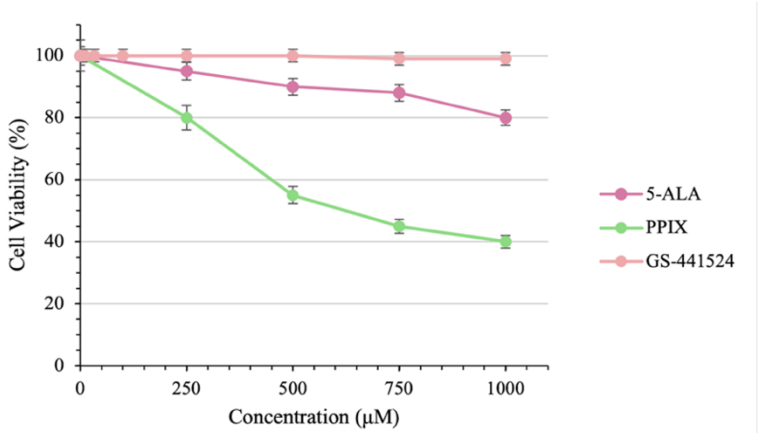

Figure 7. Cytotoxicity of 5-ALA, PPIX, and GS-441524. Data are shown as means ± SEM of three independent experiments.

with a CC_{50} around 1000 μM,[41] and PPIX may decrease cell viability at concentrations greater than 250 μM, as reported in swine kidney line-L cells.[40]

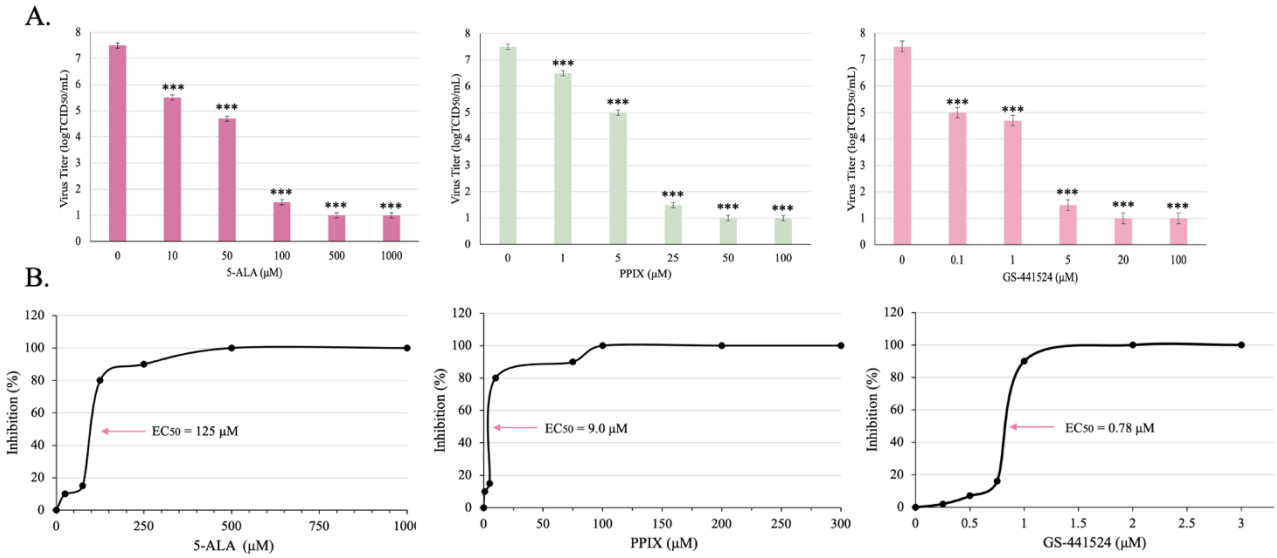

Figure 8. Inhibition of viral growth by 5-ALA and PPIX. A. Viral titers ($logTCID_{50}$/mL) and B. EC_{50} of the antiviral compounds. Data are shown as means ± SEM of three independent experiments, two-tailed Student's t-test. **P < 0.01, ***P < 0.001, ****P < 0.0001.

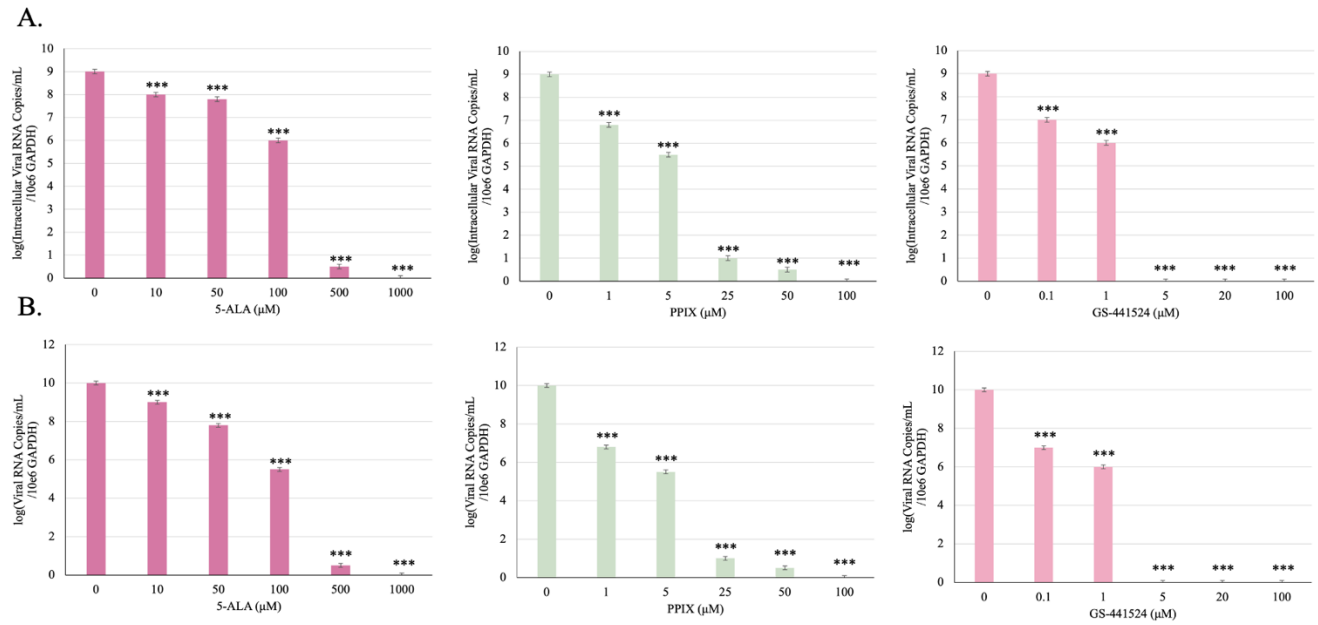

Figure 9. Viral replication is reduced by 5-ALA and PPIX. At 48 h post infection, viral RNA copies in A. cell lysates and in B. cell culture supernatants will be detected by RT-qPCR. Data are shown as means ± SEM of three independent experiments, two-tailed Student's t-test. **P < 0.01, ***P < 0.001, ****P < 0.0001.

Viral titers will be quantified by the median tissue culture infectious dose ($TCID_{50}$). It is expected that there will be a dose-dependent reduction of viral plaques by 5-ALA and PPIX. In expectation with past research,[40] PPIX should inhibit viral growth at concentrations lower than 5-ALA if it is the key antiviral compound (Figure 8A), and therefore, should display a much lower half maximal effective concentration (EC_{50}) compared to 5-ALA (Figure 8B). The antiviral activity of our compounds will also be quantified by the viral RNA copies in cell lysates and viral RNA copies in the cell culture supernatants. There should be a dose-dependent reduction of viral RNA from 5-ALA treatment, it is expected that PPIX will reduce viral copies at lower

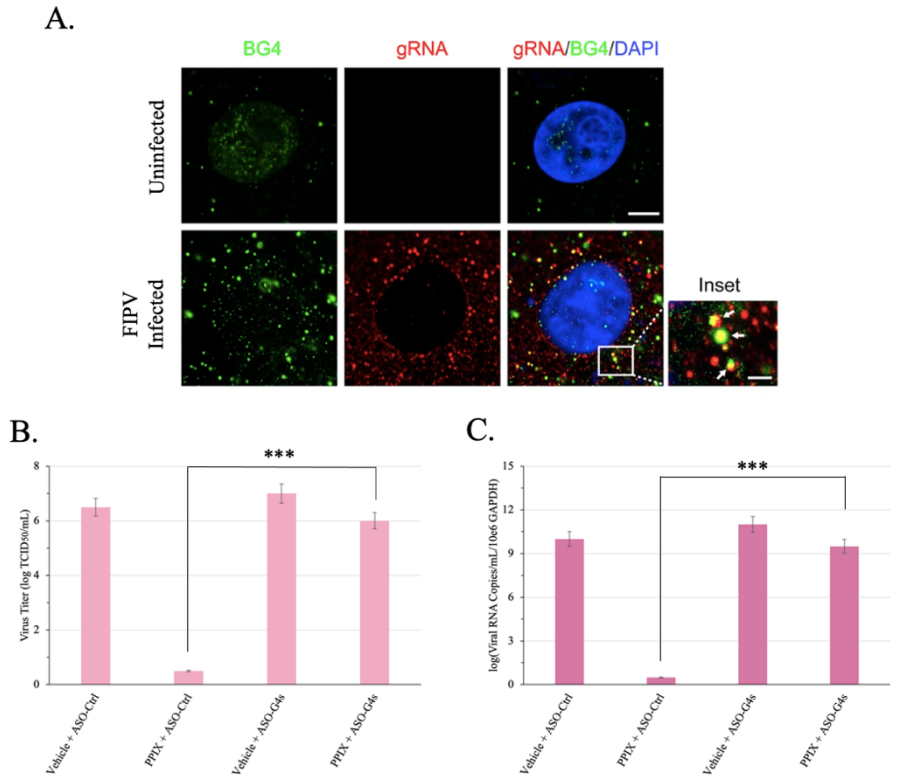

Figure 10. **LNA ASO treatment negates antiviral activity exerted by PPIX.** A. Immunofluorescence of BG4 and fluorescence in situ hybridization (FISH) for viral genomic RNA (gRNA) in CRFK cells with or without FIPV infection. Scale bars, 10 μM. Adapted from Qin et al. (2022). CRFK cells treated with 100 μM PPIX will be pre-transfected with the ASOs targeting viral G4s, and then the cells will be infected with FIPV (10^4 $TCID_{50}$ virus/mL). B. At 48 hours post infection, viral RNA copies in cell culture supernatants will be detected by RT-qPCR. C. Viral titers ($logTCID_{50}$/mL) will be quantified by $TCID_{50}$. Data are shown as means ± SEM of three independent experiments, two-tailed Student's *t*-test. $^{**}P < 0.01$, $^{***}P < 0.001$, $^{****}P < 0.0001$.

concentrations compared to 5-ALA, similar to the results from our viral titer assays (Figure 9A,9B).

It is strongly suggested from our previous results that PPIX binds the FIPV genomic RNA G4s. To confirm that viral G4 structures are in fact occurring during FIPV replication and Infection, an immunofluorescence assay employing anti-DNA/RNA G-quadruplex antibody (BG4) will be carried out. Co-localization between BG4 fluorescence and viral genomic RNA should be observed, indicating the formation of viral G4 structures during FIPV replication (Figure 10A, Adapted from Qin et al., 2022). Antisense oligonucleotides (ASOs) complementary to the X4-G4 sequence will be employed to unfold viral G4 structures in FIPV infected CRFK cells treated with PPIX. Therefore, the antiviral activity by our compounds should be significantly inhibited by the ASOs (Figure 10B, 10C).

If there are hundreds of copies of viral RNA G4s as indicated by the immunofluorescence results observed in Qin et al. (2022) (Figure 10A), this will suggest there are an outstanding amount of viral G4s in comparison to cellular G4s. Furthermore, if the antiviral effects of PPIX are achievable at the low micromolar concentrations proposed here, there is a smaller likelihood of off-target effects on host G4s. Future studies would need to explore the potential for PPIX to exert off-target effects and the resulting possible side effects.

Significance and Conclusion

This propositional study aims to extend promising research into G-quadruplex (G4) binding compounds as potential drugs for coronaviruses such as FIPV. The 5-ALA metabolite, protoporphyrin IX (PPIX), has previously been reported to demonstrate antiviral activity against a number of viruses.[43–45,47] Furthermore, 5-ALA supplementation has been shown to increase the concentration of intracellular PPIX and exert antiviral effects on Classical Swine Fever (CSF) and coronaviruses SARS-CoV-2 and FIPV.[40–42] However, these studies do not explore the mechanisms in which 5-ALA is able to inhibit viral growth in infected cells. Recently, a study investigating the antiviral mechanisms and antiviral effects of known G4-specific stabilizer TMPγP4 in SARS-CoV-2 revealed that the binding of this molecule to G4 sequences in the SARS-CoV-2 genome not only inhibits viral replication and translation, but also displays better antiviral activity than Remdesivir, an established SARS-CoV-2 therapeutic.[34] Considering that PPIX is also a known G4-specific stabilizer,[63] the data suggest that PPIX is the key player in inhibiting FIPV by binding to FIPV G4s. The prospective experiments here are designed to elucidate if PPIX is the molecule responsible for the antiviral activity demonstrated by 5-ALA treatment. If the projected results are found to be true, this would not only advance novel research into G4s as targets for antiviral drug design, but also demonstrate its ability to significantly inhibit FIPV infection in feline kidney cells. There is currently no licensed therapeutic for FIPV, and many of the drugs show poor results in cases with neurological manifestations,[21,24,64] indicating insufficient transfer across the blood brain barrier. 5-ALA is a low-molecular weight amino acid that has been shown to transfer to brain tissue.[65] Moreover, 5-ALA demonstrates high bioavailability and low cytotoxicity,[41] further implicating its potential as a therapeutic for FIPV. Results from this study will provide the basis for *in vivo* studies on infected cats, and perhaps then observe therapeutic effects in cats as well.

The possibility of a cat having FIPV poses a threat to the cat's health, causing owners to resort to black market medications.[25] Considering the demand for FIP therapies, the development of an effective and safe antiviral with few side-effects is desperately needed. GS-441542 has demonstrated rapid reversal of disease signs and recovery in cats experimentally infected with FIPV, and even entered field trials, but Gilead Sciences reportedly refused to license this drug for use in cats.[66] Not only will this research advance the possibility of 5-ALA as an effective therapeutic for cats with FIPV, but also contribute research into the novel field of G-quadruplexes as a drug target against coronaviruses like FIPV.

References

(1) Motokawa, K.; Hohdatsu, T.; Aizawa, C.; Koyama, H.; Hashimoto, H. Molecular Cloning and Sequence Determination of the Peplomer Protein Gene of Feline Infectious Peritonitis Virus Type I. *Arch. Virol.* **1995**, *140* (3), 469–480. https://doi.org/10.1007/BF01718424.

(2) Kummrow, M.; Meli, M. L.; Haessig, M.; Goenczi, E.; Poland, A.; Pedersen, N. C.; Hofmann-Lehmann, R.; Lutz, H. Feline Coronavirus Serotypes 1 and 2: Seroprevalence and Association with Disease in Switzerland. *Clin. Vaccine Immunol.* **2005**, *12* (10), 1209–1215. https://doi.org/10.1128/CDLI.12.10.1209-1215.2005.

(3) Addie, D.; Belák, S.; Boucraut-Baralon, C.; Egberink, H.; Frymus, T.; Gruffydd-Jones, T.; Hartmann, K.; Hosie, M. J.; Lloret, A.; Lutz, H.; Marsilio, F.; Pennisi, M. G.; Radford, A. D.; Thiry, E.; Truyen, U.; Horzinek, M. C. Feline Infectious Peritonitis. ABCD Guidelines on Prevention and Management. *J. Feline Med. Surg.* **2009**, *11* (7), 594–604. https://doi.org/10.1016/j.jfms.2009.05.008.

(4) Decaro, N.; Mari, V.; Lanave, G.; Lorusso, E.; Lucente, M. S.; Desario, C.; Colaianni, M. L.; Elia, G.; Ferringo, F.; Alfano, F.; Buonavoglia, C. Mutation Analysis of the Spike Protein in Italian Feline Infectious Peritonitis Virus and Feline Enteric Coronavirus Sequences. *Res. Vet. Sci.* **2021**, *135*, 15–19. https://doi.org/10.1016/j.rvsc.2020.12.023.

(5) Pedersen, N. C. A Review of Feline Infectious Peritonitis Virus Infection: 1963–2008. *J. Feline Med. Surg.* **2009**, *11* (4), 225–258. https://doi.org/10.1016/j.jfms.2008.09.008.

(6) Chang, H.-W.; Egberink, H. F.; Halpin, R.; Spiro, D. J.; Rottier, P. J. M. Spike Protein Fusion Peptide and Feline Coronavirus Virulence. *Emerg. Infect. Dis.* **2012**, *18* (7), 1089–1095. https://doi.org/10.3201/eid1807.120143.

(7) Licitra, B.; Millet, J.; Regan, A.; Hamilton, B.; Rinaldi, V.; Duhamel, G.; Whittaker, G. Mutation in Spike Protein Cleavage Site and Pathogenesis of Feline Coronavirus. *Emerg. Infect. Dis.* **2013**, *19*, 1066–1073. https://doi.org/10.3201/eid1907.121094.

(8) Gao, Y.-Y.; Wang, Q.; Liang, X.-Y.; Zhang, S.; Bao, D.; Zhao, H.; Li, S.-B.; Wang, K.; Hu, G.-X.; Gao, F.-S. An Updated Review of Feline Coronavirus: Mind the Two Biotypes. *VIRUS Res.* **2023**, *326*, 199059. https://doi.org/10.1016/j.virusres.2023.199059.

(9) Pedersen, N. C. An Update on Feline Infectious Peritonitis: Diagnostics and Therapeutics. *Vet. J. Lond. Engl. 1997* **2014**, *201* (2), 133–141. https://doi.org/10.1016/j.tvjl.2014.04.016.

(10) Pedersen, N. C.; Sato, R.; Foley, J. E.; Poland, A. M. Common Virus Infections in Cats, before and after Being Placed in Shelters, with Emphasis on Feline Enteric Coronavirus. *J. Feline Med. Surg.* **2004**, *6* (2), 83–88. https://doi.org/10.1016/j.jfms.2003.08.008.

(11) Pedersen, N. C.; Allen, C. E.; Lyons, L. A. Pathogenesis of Feline Enteric Coronavirus Infection. *J. Feline Med. Surg.* **2008**, *10* (6), 529–541. https://doi.org/10.1016/j.jfms.2008.02.006.

(12) Golovko, L.; Lyons, L. A.; Liu, H.; Sørensen, A.; Wehnert, S.; Pedersen, N. C. Genetic Susceptibility to Feline Infectious Peritonitis in Birman Cats. *Virus Res.* **2013**, *175* (1), 58–63. https://doi.org/10.1016/j.virusres.2013.04.006.

(13) Foley, J. E.; Poland, A.; Carlson, J.; Pedersen, N. C. Risk Factors for Feline Infectious Peritonitis among Cats in Multiple-Cat Environments with Endemic Feline Enteric Coronavirus. *J. Am. Vet. Med. Assoc.* **1997**, *210* (9), 1313–1318.

(14) Pedersen, N. C.; Liu, H.; Gandolfi, B.; Lyons, L. A. The Influence of Age and Genetics on Natural Resistance to Experimentally Induced Feline Infectious Peritonitis. *Vet. Immunol. Immunopathol.* **2014**, *162* (1), 33–40. https://doi.org/10.1016/j.vetimm.2014.09.001.

(15) Pedersen, N. C.; Theilen, G.; Keane, M. A.; Fairbanks, L.; Mason, T.; Orser, B.; Che, C. H.; Allison, C. Studies of Naturally Transmitted Feline Leukemia Virus Infection. *Am. J. Vet. Res.* **1977**, *38* (10), 1523–1531.
(16) Poland, A. M.; Vennema, H.; Foley, J. E.; Pedersen, N. C. Two Related Strains of Feline Infectious Peritonitis Virus Isolated from Immunocompromised Cats Infected with a Feline Enteric Coronavirus. *J. Clin. Microbiol.* **1996**, *34* (12), 3180–3184.
(17) Pedersen, N. C.; Black, J. W. Attempted Immunization of Cats against Feline Infectious Peritonitis, Using Avirulent Live Virus or Sublethal Amounts of Virulent Virus. *Am. J. Vet. Res.* **1983**, *44* (2), 229–234.
(18) Legendre, A. M.; Bartges, J. W. Effect of Polyprenyl Immunostimulant on the Survival Times of Three Cats with the Dry Form of Feline Infectious Peritonitis. *J. Feline Med. Surg.* **2009**, *11* (8), 624–626. https://doi.org/10.1016/j.jfms.2008.12.002.
(19) Bank-Wolf, B. R.; Stallkamp, I.; Wiese, S.; Moritz, A.; Tekes, G.; Thiel, H.-J. Mutations of 3c and Spike Protein Genes Correlate with the Occurrence of Feline Infectious Peritonitis. *Vet. Microbiol.* **2014**, *173* (3–4), 177–188. https://doi.org/10.1016/j.vetmic.2014.07.020.
(20) Hartmann, K.; Ritz, S. Treatment of Cats with Feline Infectious Peritonitis. *Vet. Immunol. Immunopathol.* **2008**, *123* (1), 172–175. https://doi.org/10.1016/j.vetimm.2008.01.026.
(21) Pedersen, N. C.; Perron, M.; Bannasch, M.; Montgomery, E.; Murakami, E.; Liepnieks, M.; Liu, H. Efficacy and Safety of the Nucleoside Analog GS-441524 for Treatment of Cats with Naturally Occurring Feline Infectious Peritonitis. *J. Feline Med. Surg.* **2019**, *21* (4), 271–281. https://doi.org/10.1177/1098612X19825701.
(22) Sheahan, T. P.; Sims, A. C.; Graham, R. L.; Menachery, V. D.; Gralinski, L. E.; Case, J. B.; Leist, S. R.; Pyrc, K.; Feng, J. Y.; Trantcheva, I.; Bannister, R.; Park, Y.; Babusis, D.; Clarke, M. O.; Mackman, R. L.; Spahn, J. E.; Palmiotti, C. A.; Siegel, D.; Ray, A. S.; Cihlar, T.; Jordan, R.; Denison, M. R.; Baric, R. S. Broad-Spectrum Antiviral GS-5734 Inhibits Both Epidemic and Zoonotic Coronaviruses. *Sci. Transl. Med.* **2017**, *9* (396), eaal3653. https://doi.org/10.1126/scitranslmed.aal3653.
(23) Amirian, E. S.; Levy, J. K. Current Knowledge about the Antivirals Remdesivir (GS-5734) and GS-441524 as Therapeutic Options for Coronaviruses. *One Health* **2020**, *9*, 100128. https://doi.org/10.1016/j.onehlt.2020.100128.
(24) Murphy, B. G.; Perron, M.; Murakami, E.; Bauer, K.; Park, Y.; Eckstrand, C.; Liepnieks, M.; Pedersen, N. C. The Nucleoside Analog GS-441524 Strongly Inhibits Feline Infectious Peritonitis (FIP) Virus in Tissue Culture and Experimental Cat Infection Studies. *Vet. Microbiol.* **2018**, *219*, 226–233. https://doi.org/10.1016/j.vetmic.2018.04.026.
(25) Jones, S.; Novicoff, W.; Nadeau, J.; Evans, S. Unlicensed GS-441524-Like Antiviral Therapy Can Be Effective for at-Home Treatment of Feline Infectious Peritonitis. *Anim. Open Access J. MDPI* **2021**, *11* (8), 2257. https://doi.org/10.3390/ani11082257.
(26) Ida, J.; Chan, S. K.; Glökler, J.; Lim, Y. Y.; Choong, Y. S.; Lim, T. S. G-Quadruplexes as An Alternative Recognition Element in Disease-Related Target Sensing. *Molecules* **2019**, *24* (6), 1079. https://doi.org/10.3390/molecules24061079.
(27) Ruggiero, E.; Richter, S. N. G-Quadruplexes and G-Quadruplex Ligands: Targets and Tools in Antiviral Therapy. *Nucleic Acids Res.* **2018**, *46* (7), 3270–3283. https://doi.org/10.1093/nar/gky187.
(28) Lane, A. N.; Chaires, J. B.; Gray, R. D.; Trent, J. O. Stability and Kinetics of G-Quadruplex Structures. *Nucleic Acids Res.* **2008**, *36* (17), 5482–5515. https://doi.org/10.1093/nar/gkn517.

(29) Fay, M. M.; Lyons, S. M.; Ivanov, P. RNA G-Quadruplexes in Biology: Principles and Molecular Mechanisms. *J. Mol. Biol.* **2017**, *429* (14), 2127–2147. https://doi.org/10.1016/j.jmb.2017.05.017.
(30) Rhodes, D.; Lipps, H. J. G-Quadruplexes and Their Regulatory Roles in Biology. *Nucleic Acids Res.* **2015**, *43* (18), 8627–8637. https://doi.org/10.1093/nar/gkv862.
(31) Métifiot, M.; Amrane, S.; Litvak, S.; Andreola, M.-L. G-Quadruplexes in Viruses: Function and Potential Therapeutic Applications. *Nucleic Acids Res.* **2014**, *42* (20), 12352–12366. https://doi.org/10.1093/nar/gku999.
(32) Musumeci, D.; Riccardi, C.; Montesarchio, D. G-Quadruplex Forming Oligonucleotides as Anti-HIV Agents. *Molecules* **2015**, *20* (9), 17511–17532. https://doi.org/10.3390/molecules200917511.
(33) Panera, N.; Tozzi, A. E.; Alisi, A. The G-Quadruplex/Helicase World as a Potential Antiviral Approach Against COVID-19. *Drugs* **2020**, *80* (10), 941–946. https://doi.org/10.1007/s40265-020-01321-z.
(34) Qin, G.; Zhao, C.; Liu, Y.; Zhang, C.; Yang, G.; Yang, J.; Wang, Z.; Wang, C.; Tu, C.; Guo, Z.; Ren, J.; Qu, X. RNA G-Quadruplex Formed in SARS-CoV-2 Used for COVID-19 Treatment in Animal Models. *Cell Discov.* **2022**, *8* (1), 1–13. https://doi.org/10.1038/s41421-022-00450-x.
(35) Czarnecki, O.; Grimm, B. New Insights in the Topology of the Biosynthesis of 5-Aminolevulinic Acid. *Plant Signal. Behav.* **2013**, *8* (2), e23124. https://doi.org/10.4161/psb.23124.
(36) Fujino, M.; Nishio, Y.; Ito, H.; Tanaka, T.; Li, X.-K. 5-Aminolevulinic Acid Regulates the Inflammatory Response and Alloimmune Reaction. *Int. Immunopharmacol.* **2016**, *37*, 71–78. https://doi.org/10.1016/j.intimp.2015.11.034.
(37) Yang, X.; Palasuberniam, P.; Kraus, D.; Chen, B. Aminolevulinic Acid-Based Tumor Detection and Therapy: Molecular Mechanisms and Strategies for Enhancement. *Int. J. Mol. Sci.* **2015**, *16* (10), 25865–25880. https://doi.org/10.3390/ijms161025865.
(38) Osaki, T.; Yokoe, I.; Ogura, S.; Takahashi, K.; Murakami, K.; Inoue, K.; Ishizuka, M.; Tanaka, T.; Li, L.; Sugiyama, A.; Azuma, K.; Murahata, Y.; Tsuka, T.; Ito, N.; Imagawa, T.; Okamoto, Y. Photodynamic Detection of Canine Mammary Gland Tumours after Oral Administration of 5-Aminolevulinic Acid. *Vet. Comp. Oncol.* **2017**, *15* (3), 731–739. https://doi.org/10.1111/vco.12213.
(39) Rehani, P. R.; Iftikhar, H.; Nakajima, M.; Tanaka, T.; Jabbar, Z.; Rehani, R. N. Safety and Mode of Action of Diabetes Medications in Comparison with 5-Aminolevulinic Acid (5-ALA). *J. Diabetes Res.* **2019**, *2019*, 4267357. https://doi.org/10.1155/2019/4267357.
(40) Hirose, S.; Isoda, N.; Huynh, L. T.; Kim, T.; Yoshimoto, K.; Tanaka, T.; Inui, K.; Hiono, T.; Sakoda, Y. Antiviral Effects of 5-Aminolevulinic Acid Phosphate against Classical Swine Fever Virus: In Vitro and In Vivo Evaluation. *Pathogens* **2022**, *11* (2), 164. https://doi.org/10.3390/pathogens11020164.
(41) Takano, T.; Satoh, K.; Doki, T. Possible Antiviral Activity of 5-Aminolevulinic Acid in Feline Infectious Peritonitis Virus (Feline Coronavirus) Infection. *Front. Vet. Sci.* **2021**, *8*.
(42) Sakurai, Y.; Ngwe Tun, M. M.; Kurosaki, Y.; Sakura, T.; Inaoka, D. K.; Fujine, K.; Kita, K.; Morita, K.; Yasuda, J. 5-Amino Levulinic Acid Inhibits SARS-CoV-2 Infection in Vitro. *Biochem. Biophys. Res. Commun.* **2021**, *545*, 203–207. https://doi.org/10.1016/j.bbrc.2021.01.091.

(43) Assunção-Miranda, I.; Cruz-Oliveira, C.; Neris, R. L. S.; Figueiredo, C. M.; Pereira, L. P. S.; Rodrigues, D.; Araujo, D. F. F.; Da Poian, A. T.; Bozza, M. T. Inactivation of Dengue and Yellow Fever Viruses by Heme, Cobalt-Protoporphyrin IX and Tin-Protoporphyrin IX. *J. Appl. Microbiol.* **2016**, *120* (3), 790–804. https://doi.org/10.1111/jam.13038.
(44) Cruz-Oliveira, C.; Almeida, A. F.; Freire, J. M.; Caruso, M. B.; Morando, M. A.; Ferreira, V. N. S.; Assunção-Miranda, I.; Gomes, A. M. O.; Castanho, M. A. R. B.; Da Poian, A. T. Mechanisms of Vesicular Stomatitis Virus Inactivation by Protoporphyrin IX, Zinc-Protoporphyrin IX, and Mesoporphyrin IX. *Antimicrob. Agents Chemother.* **2017**, *61* (6), e00053-17. https://doi.org/10.1128/AAC.00053-17.
(45) Neris, R. L. S.; Figueiredo, C. M.; Higa, L. M.; Araujo, D. F.; Carvalho, C. A. M.; Verçoza, B. R. F.; Silva, M. O. L.; Carneiro, F. A.; Tanuri, A.; Gomes, A. M. O.; Bozza, M. T.; Da Poian, A. T.; Cruz-Oliveira, C.; Assunção-Miranda, I. Co-Protoporphyrin IX and Sn-Protoporphyrin IX Inactivate Zika, Chikungunya and Other Arboviruses by Targeting the Viral Envelope. *Sci. Rep.* **2018**, *8* (1), 9805. https://doi.org/10.1038/s41598-018-27855-7.
(46) Ma, L.-L.; Zhang, P.; Wang, H.-Q.; Li, Y.-F.; Hu, J.; Jiang, J.-D.; Li, Y.-H. Heme Oxygenase-1 Agonist CoPP Suppresses Influenza Virus Replication through IRF3-Mediated Generation of IFN-α/β. *Virology* **2019**, *528*, 80–88. https://doi.org/10.1016/j.virol.2018.11.016.
(47) Gu, C.; Wu, Y.; Guo, H.; Zhu, Y.; Xu, W.; Wang, Y.; Zhou, Y.; Sun, Z.; Cai, X.; Li, Y.; Liu, J.; Huang, Z.; Yuan, Z.; Zhang, R.; Deng, Q.; Qu, D.; Xie, Y. Protoporphyrin IX and Verteporfin Potently Inhibit SARS-CoV-2 Infection in Vitro and in a Mouse Model Expressing Human ACE2. *Sci. Bull.* **2021**, *66* (9), 925–936. https://doi.org/10.1016/j.scib.2020.12.005.
(48) Weitner, T.; Kos, I.; Sheng, H.; Tovmasyan, A.; Reboucas, J. S.; Fan, P.; Warner, D. S.; Vujaskovic, Z.; Batinic-Haberle, I.; Spasojevic, I. Comprehensive Pharmacokinetic Studies and Oral Bioavailability of Two Mn Porphyrin-Based SOD Mimics, MnTE-2-PyP5+ and MnTnHex-2-PyP5+. *Free Radic. Biol. Med.* **2013**, *58*, 73–80. https://doi.org/10.1016/j.freeradbiomed.2013.01.006.
(49) Kabbara, A.; Vialet, B.; Marquevielle, J.; Bonnafous, P.; Mackereth, C. D.; Amrane, S. RNA G-Quadruplex Forming Regions from SARS-2, SARS-1 and MERS Coronoviruses. *Front. Chem.* **2022**, *10*, 1014663. https://doi.org/10.3389/fchem.2022.1014663.
(50) Amrane, S.; Kerkour, A.; Bedrat, A.; Vialet, B.; Andreola, M.-L.; Mergny, J.-L. Topology of a DNA G-Quadruplex Structure Formed in the HIV-1 Promoter: A Potential Target for Anti-HIV Drug Development. *J. Am. Chem. Soc.* **2014**, *136* (14), 5249–5252. https://doi.org/10.1021/ja501500c.
(51) Garant, J.-M.; Perreault, J.-P.; Scott, M. S. Motif Independent Identification of Potential RNA G-Quadruplexes by G4RNA Screener. *Bioinformatics* **2017**, *33* (22), 3532–3537. https://doi.org/10.1093/bioinformatics/btx498.
(52) Garant, J.-M.; Perreault, J.-P.; Scott, M. S. G4RNA Screener Web Server: User Focused Interface for RNA G-Quadruplex Prediction. *Biochimie* **2018**, *151*, 115–118. https://doi.org/10.1016/j.biochi.2018.06.002.
(53) McKeirnan, A. J.; Evermann, J. F.; Davis, E. V.; Ott, R. L. Comparative Properties of Feline Coronaviruses in Vitro. *Can. J. Vet. Res.* **1987**, *51* (2), 212–216.
(54) Kikin, O.; D'Antonio, L.; Bagga, P. S. QGRS Mapper: A Web-Based Server for Predicting G-Quadruplexes in Nucleotide Sequences. *Nucleic Acids Res.* **2006**, *34* (suppl_2), W676–W682. https://doi.org/10.1093/nar/gkl253.

(55) Beaudoin, J.-D.; Jodoin, R.; Perreault, J.-P. New Scoring System to Identify RNA G-Quadruplex Folding. *Nucleic Acids Res.* **2014**, *42* (2), 1209–1223. https://doi.org/10.1093/nar/gkt904.
(56) Bedrat, A.; Lacroix, L.; Mergny, J.-L. Re-Evaluation of G-Quadruplex Propensity with G4Hunter. *Nucleic Acids Res.* **2016**, *44* (4), 1746–1759. https://doi.org/10.1093/nar/gkw006.
(57) Kreig, A.; Calvert, J.; Sanoica, J.; Cullum, E.; Tipanna, R.; Myong, S. G-Quadruplex Formation in Double Strand DNA Probed by NMM and CV Fluorescence. *Nucleic Acids Res.* **2015**, *43* (16), 7961–7970. https://doi.org/10.1093/nar/gkv749.
(58) Dye, C.; Siddell, S. G. Genomic RNA Sequence of Feline Coronavirus Strain FIPV WSU-79/1146. *J. Gen. Virol.* **2005**, *86* (Pt 8), 2249–2253. https://doi.org/10.1099/vir.0.80985-0.
(59) Camero, M.; Lanave, G.; Catella, C.; Lucente, M. S.; Sposato, A.; Mari, V.; Tempesta, M.; Martella, V.; Buonavoglia, A. ERDRP-0519 Inhibits Feline Coronavirus in Vitro. *BMC Vet. Res.* **2022**, *18* (1), 55. https://doi.org/10.1186/s12917-022-03153-3.
(60) Wang, S.-R.; Min, Y.-Q.; Wang, J.-Q.; Liu, C.-X.; Fu, B.-S.; Wu, F.; Wu, L.-Y.; Qiao, Z.-X.; Song, Y.-Y.; Xu, G.-H.; Wu, Z.-G.; Huang, G.; Peng, N.-F.; Huang, R.; Mao, W.-X.; Peng, S.; Chen, Y.-Q.; Zhu, Y.; Tian, T.; Zhang, X.-L.; Zhou, X. A Highly Conserved G-Rich Consensus Sequence in Hepatitis C Virus Core Gene Represents a New Anti–Hepatitis C Target. *Sci. Adv.* **2016**, *2* (4), e1501535. https://doi.org/10.1126/sciadv.1501535.
(61) Li, Q.; Yi, D.; Lei, X.; Zhao, J.; Zhang, Y.; Cui, X.; Xiao, X.; Jiao, T.; Dong, X.; Zhao, X.; Zeng, H.; Liang, C.; Ren, L.; Guo, F.; Li, X.; Wang, J.; Cen, S. Corilagin Inhibits SARS-CoV-2 Replication by Targeting Viral RNA-Dependent RNA Polymerase. *Acta Pharm. Sin. B* **2021**, *11* (6), 1555–1567. https://doi.org/10.1016/j.apsb.2021.02.011.
(62) Min, J. S.; Kim, G.-W.; Kwon, S.; Jin, Y.-H. A Cell-Based Reporter Assay for Screening Inhibitors of MERS Coronavirus RNA-Dependent RNA Polymerase Activity. *J. Clin. Med.* **2020**, *9* (8), 2399. https://doi.org/10.3390/jcm9082399.
(63) Li, T.; Wang, E.; Dong, S. Parallel G-Quadruplex-Specific Fluorescent Probe for Monitoring DNA Structural Changes and Label-Free Detection of Potassium Ion. *Anal. Chem.* **2010**, *82* (18), 7576–7580. https://doi.org/10.1021/ac1019446.
(64) Kameshima, S.; Kimura, Y.; Doki, T.; Takano, T.; Park, C.-H.; Itoh, N. Clinical Efficacy of Combination Therapy of Itraconazole and Prednisolone for Treating Effusive Feline Infectious Peritonitis. *J. Vet. Med. Sci.* **2020**, *82* (10), 1492–1496. https://doi.org/10.1292/jvms.20-0049.
(65) Novotny, A.; Xiang, J.; Stummer, W.; Teuscher, N. S.; Smith, D. E.; Keep, R. F. Mechanisms of 5-Aminolevulinic Acid Uptake at the Choroid Plexus. *J. Neurochem.* **2000**, *75* (1), 321–328. https://doi.org/10.1046/j.1471-4159.2000.0750321.x.
(66) *FIP research: New hope for cats (and maybe humans)*. https://www.aaha.org/publications/newstat/articles/2022-11/fip-research-new-hope-for-cats-and-maybe-humans/ (accessed 2023-11-14).

Appendix

Table S1. Characteristics of the 24 putative G-quadruplexes.

PQS	Position[a]	Gene[a]	Sequences	cGcC[b]	G4H[c]	G4NN[d]
P1	172	-	GGAACGGGGTTGAGA GAACGGCGCACCAGG	**4.5**	0.8	**0.5039**
B2	1053	ORF1a-nsp2	GGTGTTGGTGATTGGA CTGG	**18**	0.85	**0.6573**
P3	2441	ORF1a-nsp2	GGAATTGGATTTTGGT GCCATCTGG	3.4	0.48	0.0094
P4	5145	ORF1a-nsp3	GGTCCTGTGGTAGCG GCACCTCTTTTGG	1.6364	0.25	0.0061
P5	8010	ORF1a-nsp4	GGTTTTTGCTTCGGTG GCGACAACTGG	3.6	0.4815	0.0023
P6	8828	ORF1a-nsp5	GGAACCCTGTATTGTA AGGGTGGCTTATGG	2.1818	0.4333	0.0232
P7	9281	ORF1a-nsp5	GGAATTAGGTAATGG TTCTCATGTTGG	**8.5**	0.5556	0.4796
P8	10536	ORF1a-nsp6	GGCATTGGTGGAGG	**16**	**1.0714**	**0.5761**
P9	11493	ORF1a-nsp9	GGTAAAGCGCTTATG GCTTCTGAAGGTGG	**4.75**	0.5172	0.0829
P10	11886	ORF1a-nsp10	GGTGCCGGTAATGGT ATGG	4.25	0.6842	0.0437
P11	14171	ORF1b	GGTGGTACAACTAGT GGTGATGG	**9**	0.6957	**0.5052**
P12	15400	ORF1b	GGAGGTTATCGGCCCT AAGG	1.4545	0.3	0.022
P13	19243	ORF1b	GGCATGGAGATGGAT GCTGTGG	**9.5**	0.7727	**0.543**
P14	20119	ORF1b	GGTCGTTGGATTACTA AGGAAGGG	**11.5**	0.8333	**0.833**
P15	20374	S	GGTGGTTATTACCCTA CAGAGGTGTGG	1.6364	0.2963	0.0144
P16	23026	S	GGTTCTTGGCTAGGAG G	**8**	0.8235	0.4494
P17	23296	S	GGTGCACTTGGTGGTG GCGCCGTGG	3.2857	0.64	0.4817
P18	23431	S	GGTAACATTACACAG GCTTTTGGTAAGG	4	0.4286	0.0376
P19	24380	S	GGCCTTGGTATGTGTG GCTACTGATAGG	3.1667	0.4643	0.0982
P20	24460	S	GGTTGTTGTGGATGCA TAGGTTGTTTAGG	**20**	0.6552	**0.7277**

P21	26548	M	GGTTTCAAAATGGCTG GTGG	**8**	0.7	0.0185
P22	26962	N	GGTAATAAGGATCAA CAAATTGGTTATTGG	**8**	0.466 7	0.1667
P23	27022	N	GGCCAGCGTAAGGAA CTCGCTGAGAGGTGG	2.625	0.433 3	0.1945
P24	27112	N	GGAGTCTTCTGGGTTG CAAGGGATGG	**10**	**0.961 5**	**0.8589**

[a]Positions and genes are based on FIPV 79-1146 complete genome.[58] [b]GcCc (the consecutive G over consecutive C ratio) addresses the issue of competition between G4 and Watson-Crick based structures, and the threshold value is 4.5. [c]G4H (G4Hunter) analyzes DNA sequences in which each contiguous G receives an increasing positive score, and each contiguous C receives an increasing negative score, with the average of these values producing a final score. The threshold is 0.9. G4NN (G4 neural network) is an artificial neural network that compares the similarity of the given sequence to known G-quadruplexes and reports it as a score between 0 and 1. The threshold is 0.5. ORF, open reading frame; S, spike glycoprotein; M, membrane protein; N, nucleocapsid protein. Boldface type indicates that the scores of putative G-quadruplexes are above the threshold.